

See discussions, stats, and author profiles for this publication at: <https://www.researchgate.net/publication/370442241>

# Smoothed particle hydrodynamics method for pinch plasma simulation with non-ideal MHD Model

Article in Physics of Plasma · May 2023

DOI: 10.1063/5.0138221

---

CITATIONS

2

READS

244

1 author:



Park Su-San  
Seoul National University

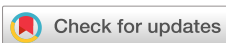
7 PUBLICATIONS 41 CITATIONS

[SEE PROFILE](#)

RESEARCH ARTICLE | MAY 01 2023

## Smoothed particle hydrodynamics method for pinch plasma simulation with non-ideal MHD model

Su-San Park; Deok-Kyu Kim; Jin-Hyun Kim; ... et. al



*Physics of Plasmas* 30, 053901 (2023)

<https://doi.org/10.1063/5.0138221>

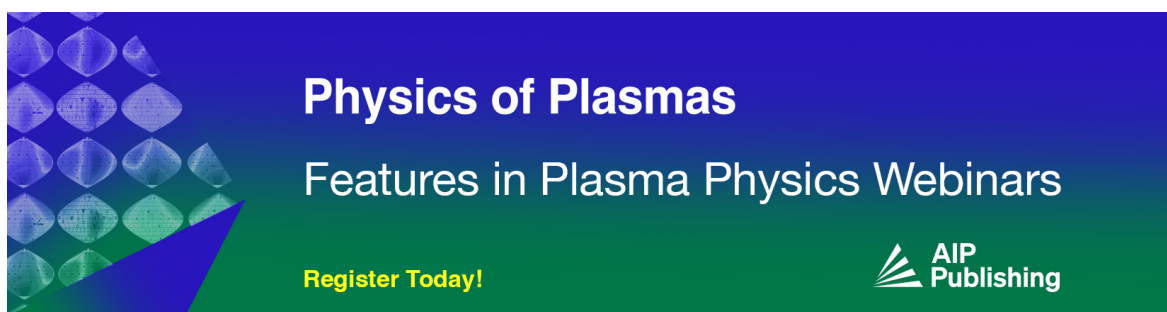


View  
Online



Export  
Citation

CrossMark



The banner features a blue gradient background with a grid of glowing blue plasma filaments on the left. The text "Physics of Plasmas" is at the top, followed by "Features in Plasma Physics Webinars". A "Register Today!" button is at the bottom left, and the AIP Publishing logo is at the bottom right.

Physics of Plasmas

Features in Plasma Physics Webinars

Register Today!

AIP Publishing

# Smoothed particle hydrodynamics method for pinch plasma simulation with non-ideal MHD model

Cite as: Phys. Plasmas **30**, 053901 (2023); doi: [10.1063/5.0138221](https://doi.org/10.1063/5.0138221)

Submitted: 9 December 2022 · Accepted: 8 April 2023 ·

Published Online: 1 May 2023



View Online



Export Citation



CrossMark

Su-San Park,<sup>1,a)</sup> Deok-Kyu Kim,<sup>2</sup> Jin-Hyun Kim,<sup>1</sup> and Eung Soo Kim<sup>1,b)</sup>

## AFFILIATIONS

<sup>1</sup>Department of Nuclear Engineering, Seoul National University, Seoul 08826, South Korea

<sup>2</sup>Agency for Defense Development, Daejeon 34186, South Korea

<sup>a)</sup>[michle11@snu.ac.kr](mailto:michle11@snu.ac.kr)

<sup>b)</sup>Author to whom correspondence should be addressed: [kes7741@snu.ac.kr](mailto:kes7741@snu.ac.kr)

## ABSTRACT

When plasma is compressed by magnetic forces, a pinch phenomenon is observed. Pinch plasma has received significant attention as an efficient source of radiation and a way for high-density plasma physics analysis. In this study, a non-ideal magnetohydrodynamics (MHD) model is applied to a smoothed particle hydrodynamics (SPH) framework to analyze pinch plasmas whose local resistivity varies with temperature and pressure. The proposed SPH model incorporates several numerical treatments, such as a correction term to satisfy the  $\nabla \cdot \mathbf{B}$  constraint and some artificial dissipation terms to govern the shock wave. Moreover, it includes the evaluation of a novel SPH discretization for non-ideal MHD terms, including current density calculations. Furthermore, the proposed model is validated with three benchmark cases: (1) Brio and Wu shock tube (ideal MHD), (2) resistive MHD shock simulation, and (3) magnetized Noh Z-pinch problem. The simulation results are compared with the results of some reference Eulerian MHD simulations and analytical solutions. The simulations agree well with the reference data, and the introduced numerical treatments are effective. Finally, X-pinch simulations are performed using the proposed model. The simulations well produce the micro Z-pinch and jet shapes, which are important X-pinch features. Overall, the proposed SPH model has extensive potential for studying the complex pinch plasma phenomena.

Published under an exclusive license by AIP Publishing. <https://doi.org/10.1063/5.0138221>

## I. INTRODUCTION

A pinch is a phenomenon that occurs in plasma when it is compressed by magnetic forces. Recently, pinch plasma has received considerable attention as an efficient source of radiation and a method for high-density plasma physics analysis.<sup>1–3</sup> However, the experimental implementation of pinch plasma is difficult as it requires high-performance current sources and various diagnostic equipment. Thus, various numerical approaches have been proposed to describe the complex behavior of pinch plasmas, and among them, magnetohydrodynamics (MHD) simulation is a powerful tool. The resistive MHD model has been used to describe plasmas whose local resistivity varies with temperature and pressure.<sup>4,5</sup> This model accurately captures the rapid changes in pinch plasma behavior.

Multi-dimensional resistive MHD codes, such as FLASH, MARE2D, ZEUS, and ATHENA, have been utilized to study the magnetized Noh Pinch problem and the implosion evolution of simple wire-array Z-pinch.<sup>5–9</sup> The Eulerian modular code PLUTO<sup>4,10–12</sup>

was recently used to simulate the plasma dynamics of X-pinch experiments with two tungsten wires.<sup>13</sup> Particularly, the GORGON code has been determined to be ideal for MHD plasma applications involving X- and Z-pinch wire configurations.<sup>14–17</sup>

Although Eulerian codes are widely used to simulate pinch plasmas under extreme conditions, they require additional numerical processes to handle complex and deformable boundaries due to their reliance on pre-defined and fixed meshes. In contrast, Lagrangian numerical methods allow physical fields to move along with particles and are relatively free from such problems. Therefore, they can yield more compact expressions for MHD calculations performed at the boundary between plasma and vacuum.

Smoothed particle hydrodynamics (SPH) is a Lagrangian-based particle method for solving fluid dynamics equations. Since it was first proposed by Monaghan in the late 1970s,<sup>18</sup> it has been employed to simulate various MHD scenarios. In 2012, Tricco and Price proposed a smoothed particle MHD (SPMHD) scheme that incorporates the

hyperbolic divergence cleaning method.<sup>19</sup> They improved the existing method of Price and Monaghan<sup>20</sup> by altering the discretization forms for  $\nabla \cdot \mathbf{B}$  and  $\nabla \varphi$ . Iwasaki proposed an SPMHD method based on the Godunov SPH proposed by Inutsuka.<sup>21,22</sup> Instead of employing the artificial dissipation term used in Price and Monaghan, Iwasaki used a solution of the non-linear Riemann problem to reduce the numerical dissipation. Tsukamoto suggested an SPH discretization of Ohmic dissipation,<sup>23</sup> and Vela extended it to the pinch plasma problem through a new boundary treatment method.<sup>24</sup> However, the previously proposed SPMHD methodologies do not afford a consistent SPH discretization for non-ideal MHD terms. Furthermore, pinch plasma constitutes extreme conditions of high temperature of over  $10^6$  K and high density of over  $10^3$  kg/m<sup>3</sup>, which have not been analyzed in previous studies. A novel process is required to obtain and verify the SPH discretization suitable for pinch plasma simulations under extreme conditions.

In this study, the non-ideal MHD model is developed and implemented to the SPH framework. The model is based on the existing SPH-based hydrodynamics code,<sup>25</sup> but it includes some additional calculations that are essential for analyzing pinch plasmas, such as the magnetic pressure force and the resistive induction equation. In addition, this model incorporates various numerical techniques for capturing shock or reducing the numerical instability proposed in previous SPMHD studies. Specifically, a novel SPH discretization for the non-ideal MHD term is proposed that can be employed in the extreme conditions of pinch plasmas. Finally, some benchmark problems are simulated to validate the proposed SPH code.

The rest of this paper is organized as follows: The resistive MHD governing equations used for the pinch plasma simulation are given in Sec. II. Section III presents the numerical method, including the new SPH discretization for the non-ideal MHD terms and the SPH techniques for improving the numerical accuracy. In Sec. IV, the numerical method is tested using three different numerical examples and is used for X-pinch simulation. The conclusions and suggestions are presented in Sec. V.

## II. GOVERNING EQUATION

### A. Resistive MHD equations

MHD is the study of the magnetic properties and behavior of electrically conducting fluids, specifically plasmas. Plasma is a state of matter that comprises charged particles, such as ions and electrons. In principle, to describe plasma behavior, the equation of motion of each particle needs to be calculated. However, since plasma contains abundant particles, solving the equations of motion for each particle is impractical. Instead, MHD equations are derived by treating the plasma as a continuum, where the fluid is assumed to have the same properties at each unit domain.<sup>26</sup> This simplification allows for a more tractable description of plasma behavior and has been proven to be a powerful tool for understanding and predicting plasma dynamics. The MHD equations are a combination of the Navier–Stokes equations of fluid dynamics and Maxwell's equations of electromagnetism. These differential equations need to be simultaneously solved, either analytically or numerically. Various MHD equations can be derived depending on the type of plasma and applied assumptions. The MHD equations used herein are the resistive MHD equations that include the effect of plasma resistivity in ideal MHD. In this section, the governing equations constituting the MHD equations are described.

The main variables characterizing an electrically conductive fluid are the bulk plasma velocity field  $v$ , internal energy  $u$ , mass density  $\rho$ ,

and thermodynamic pressure  $P$ . The flowing charged particles are the source of the magnetic field  $\mathbf{B}$ , electric field  $\mathbf{E}$ , and current density  $\mathbf{J}$ . All these parameters generally vary with time  $t$ . By neglecting the displacement current, plasma viscosity, and thermal conduction, the equations based on the resistive MHD model can be expressed using the Lagrangian derivative  $d/dt = \partial/\partial t + \mathbf{v} \cdot \nabla$ , shown as follows:<sup>27</sup>

$$\frac{d\rho}{dt} + \rho(\nabla \cdot \mathbf{v}) = 0, \quad (1)$$

$$\frac{d\mathbf{v}}{dt} = \frac{1}{\rho} \nabla \cdot \left( \frac{\mathbf{B} \otimes \mathbf{B}}{\mu_0} - \left( \frac{|\mathbf{B}|^2}{2\mu_0} + P \right) \vec{I} \right), \quad (2)$$

$$\frac{d\mathbf{B}}{dt} = -\mathbf{B}(\nabla \cdot \mathbf{v}) + (\mathbf{B} \cdot \nabla)\mathbf{v} - \nabla \times \eta \mathbf{J}, \quad (3)$$

$$\frac{du}{dt} = -\frac{P}{\rho}(\nabla \cdot \mathbf{v}) + \frac{\eta |\mathbf{J}|^2}{\rho}, \quad (4)$$

where the current density  $\mathbf{J}$  is obtained as follows according to Ampère's law

$$\mathbf{J} = \frac{1}{\mu_0} \nabla \times \mathbf{B}. \quad (5)$$

### B. Equations of state

The above governing equations are closed by the equation of state (EOS), which determines the fluid pressure as a function of density and internal energy. For accurate hydrodynamic simulations, the EOS model should be chosen as it yields accurate thermodynamic properties of a matter over a wide range of relevant physical conditions.

The ideal gas EOS is the simplest EOS and can be easily and quickly incorporated in MHD simulations despite its restrictions on the valid physical conditions,

$$P = (\gamma - 1)\rho u, \quad (6)$$

where  $\gamma = C_p/C_v$  is the adiabatic index,  $C_v$  is the specific heat at constant volume, and  $C_p$  is the specific heat at constant pressure.

Various EOS models that are practically applicable to real materials have been developed based on fundamental thermodynamic and statistical physics, such as the chemical equilibrium model of Saha equation<sup>28,29</sup> and the Thomas–Fermi theory of quotidian equation of state (QEOS).<sup>30</sup> In this study, EOS data tables for high-energy-density (HED) plasma conditions are constructed using theoretical approaches mainly based on the Thomas–Fermi theory, and the average ionization degree is computed by the fitted formula given by the Lee–More model.<sup>31</sup> The EOS table is implemented in the novel SPH code to simulate plasma discharges in X-pinch configurations.

To verify the SPH code performance validation by comparing benchmark solutions, the same ideal gas EOS as in other researchers' calculations is used. However, the real material EOS data table is applied in the SPH simulation of X-pinch plasmas; thus, the results are presented in comparison with image shots available from the preliminary experiments at Seoul National University (SNU).

## III. NUMERICAL METHODS

### A. Basic formulations of the SPH method

In the SPH method, the entire fluid system is expressed by a finite number of particles representing the material properties of that space,

and physical quantities, such as density, momentum, and internal energy, are determined by the smoothing of neighboring particles. The smoothing procedure in the SPH method is based on the theory of integral interpolants using a delta function,

$$f(r) = \int_{\Omega} f(r') \delta(r - r', h) d\Omega. \quad (7)$$

However, the delta function is difficult to numerically handle as it is a discontinuous function. To solve this problem, the delta function can be approximated to a continuous function  $W$  (known as the smoothing kernel function) with a characteristic width  $h$  (known as the smoothing length). The integral interpolant of a function  $f$  is defined as follows:<sup>18</sup>

$$f(r) = \int_{\Omega} f(r') W(r - r', h) d\Omega. \quad (8)$$

The integral form of Eq. (8) can be discretized by representing the integral with a summation expression, and it ensures the second-order accuracy for  $h$ ,

$$\langle f(\mathbf{r}_i) \rangle = \sum_j f_j W(\mathbf{r}_i - \mathbf{r}_j, h) \frac{m_j}{\rho_j}, \quad (9)$$

where  $f(\mathbf{r}_i)$  is a function at the position  $\mathbf{r}_i$ , the subscript  $j$  denotes the particles near the center particle  $i$ , and  $m/\rho$  is the particle volume. Given that  $W$  is differentiable, a discrete approximation to the interpolated gradient of  $f(\mathbf{r}_i)$  can be similarly found by

$$\langle \nabla f(\mathbf{r}_i) \rangle = \sum_j f_j \nabla W(\mathbf{r}_i - \mathbf{r}_j, h) \frac{m_j}{\rho_j}. \quad (10)$$

Based on this expression, various types of SPH discretization can be induced, and the following symmetric formulation is generally used to preserve the physical quantities,

$$\langle \nabla f(\mathbf{r}_i) \rangle = \rho_i \sum_j m_j \left[ \frac{f_i}{\rho_i^2} + \frac{f_j}{\rho_j^2} \right] \nabla W(\mathbf{r}_i - \mathbf{r}_j, h). \quad (11)$$

To apply the kernel function  $W$  as an averaging weighting function in the SPH method, it must satisfy some mathematical properties of the delta function.<sup>32</sup> The first condition is the “unity condition,” which means that the integral value over the entire volume should have the value of one, which is the same as the delta function. In addition, since calculations for an infinite area are impossible to perform, the value of the kernel function must be zero outside the support domain (compact condition) and must always be positive within the support domain (positive condition). Furthermore, the other conditions that must be satisfied are the “decay condition,” which requires that the kernel function value should monotonically decrease with increasing distance from the reference particle; the “delta function condition,” which requires that the function becomes identical to the Dirac delta function as  $h$  approaches zero; and the “symmetric condition,” which requires the kernel function to be symmetric. The conditions are summarized in Table I.

In previous SPH studies, various kinds of kernel functions that satisfy these properties have been proposed. This study employs the

**TABLE I.** Conditions of kernel function.

Condition	Mathematical expression
Unity condition	$\int_{\Omega} W(r, h) d\Omega = 1$
Symmetry condition	$W(r, h) = W(-r, h)$
Delta-function approximation	$\lim_{h \rightarrow 0} W(r, h) = \delta(r)$
Compact support condition	$W(r, h) = 0$ for $ r  > \kappa h$
Positive condition	$W(r, h) \geq 0$ for any $r$
Monotonic decrease condition	$W'(r, h) < 0$

Wendland kernel function, which prevents particle clustering by performing a non-negative Fourier transform in the multi-dimensional analysis:<sup>33</sup>

$$W(R^*, h) = \begin{cases} \frac{5}{4(2h)} (1 - R^*)^3 (1 + 3R^*) & 1D \\ \frac{7}{\pi(2h)^2} (1 - R^*)^4 (1 + 4R^*) & 2D \\ \frac{21}{2\pi(2h)^3} (1 - R^*)^4 (1 + 4R^*) & 3D. \end{cases} \quad (12)$$

## B. SPH formulation for resistive MHD

Applying the SPH formulation for the differential operator described earlier, the resistive MHD governing equations, comprising the continuity equation Eq. (13), momentum equation Eq. (14), induction equation Eq. (15), energy equation Eq. (16), and EOS Eq. (17), are as follows:

$$\rho_i = m_i \sum_j W_{ij}, \quad (13)$$

$$\frac{d\mathbf{v}_i}{dt} = \sum_j m_j \left( \frac{\vec{M}_i}{\rho_i^2} + \frac{\vec{M}_j}{\rho_j^2} \right) \cdot \nabla_i W_{ij}, \quad (14)$$

$$\frac{d\mathbf{B}_i}{dt} = \frac{1}{\rho_i} \sum_j m_j (\mathbf{B}_i \mathbf{v}_{ij} - \mathbf{v}_{ij} \mathbf{B}_i) \cdot \nabla_i W_{ij} + \left( \frac{dB_i}{dt} \right)_{\text{non-ideal}}, \quad (15)$$

$$\frac{du_i}{dt} = \frac{1}{2} \sum_j m_j \left( \frac{P_i}{\rho_i^2} + \frac{P_j}{\rho_j^2} \right) \mathbf{v}_{ij} \cdot \nabla_i W_{ij} + \frac{1}{\rho_i} \eta J_i^2, \quad (16)$$

$$P_i = P(u_i, \rho_i), \quad (17)$$

where  $\vec{M} = \mathbf{B}\mathbf{B} - (\mathbf{B}^2/2 + P)\vec{I}$  is the Maxwell stress tensor,  $\mathbf{v}_{ij} = \mathbf{v}_i - \mathbf{v}_j$  is the relative velocity between two particles, and  $W_{ij} = W(\mathbf{r}_i - \mathbf{r}_j, h)$  denotes the kernel function. For this implementation, a unit for the magnetic field is used that normalizes the permeability  $\mu_0$  to 1 in the same way as some previous MHD studies.<sup>34–36</sup>

## C. Numerical techniques of the SPH method

The SPH simulation for pinch plasmas has various features that threaten the numerical stability and accuracy. In this section, several characteristics of pinch plasmas that lead to inaccurate SPH calculation are discussed and additional numerical terms for eliminating these inaccuracies are introduced.

According to Gauss's law for magnetism, magnetic monopoles cannot exist. Thus, the magnetic field line is always a closed curve, and  $\nabla \cdot \mathbf{B}$  is always zero. However, in numerical MHD simulations,  $\nabla \cdot \mathbf{B}$  is not accurately zero because of numerical noise. The approach of Børve explicitly negates the effect of the non-vanishing  $\nabla \cdot \mathbf{B}$  by adding a corrective term to the momentum equation,<sup>37</sup>

$$\left(\frac{d\mathbf{v}}{dt}\right)_{\nabla \cdot \mathbf{B}} = -\mathbf{B}_i \sum_j m_j \left(\frac{\mathbf{B}_i}{\rho_i^2} + \frac{\mathbf{B}_j}{\rho_j^2}\right) \cdot \nabla W_{ij}. \quad (18)$$

Early shock simulation studies recognized that a shock wave accompanied by a sharp velocity discontinuity boundary results in inaccurate calculations during numerical simulations. Some researchers widened the transition zone to computationally resolve the discontinuous boundary by introducing an unphysical viscosity, called "artificial viscosity".<sup>38,39</sup> Various types of artificial viscosity have been proposed and developed in different numerical schemes over the past several decades. In this study, the artificial viscosity form commonly used in SPH methodology is employed to resolve the discontinuous boundaries that occur during plasma compression. It is an improved version of the artificial viscosity introduced by Monaghan and Gingold,<sup>40</sup>

$$\left(\frac{d\mathbf{v}_i}{dt}\right)_{diss} = -\sum_j m_j \Pi_{ij} \nabla_i W_{ij},$$

$$\Pi_{ij} = \begin{cases} \frac{-\alpha \bar{c}_{ij} \phi_{ij} + \beta \phi_{ij}^2}{\bar{\rho}_{ij}} & \text{if } (\mathbf{v}_{ij} \cdot \mathbf{r}_{ij} < 0) \\ 0 & \text{if } (\mathbf{v}_{ij} \cdot \mathbf{r}_{ij} \geq 0) \end{cases}, \quad \text{where } \phi_{ij} = \frac{h_{ij} \mathbf{v}_{ij} \cdot \mathbf{r}_{ij}}{|\mathbf{r}_{ij}|^2 + \varphi^2}, \quad (19)$$

where  $\alpha$  and  $\beta$  are constants that are typically set as approximately 1.0, and  $\varphi = 0.1 h_{ij}$  is applied to prevent numerical divergences. Here,  $h_{ij}$  represents the average smoothing length between particles  $i$  and  $j$ , while  $\bar{\rho}_{ij}$  and  $\bar{c}_{ij}$  are the mean density and speed of sound between particles  $i$  and  $j$ , respectively. The distance between particles  $i$  and  $j$  is denoted as  $r_{ij}$ . To conserve the total energy, the work done needs to be compensated for against the viscous force, shown as follows:

$$\left(\frac{du}{dt}\right)_{diss} = \frac{1}{2} \sum_j m_j \Pi_{ij} \mathbf{v}_{ij} \cdot \nabla_i W_{ij}. \quad (20)$$

In MHD simulations, shocks can lead to discontinuities in the magnetic field, which induce numerical instability. To address this issue, artificial resistivity can be introduced, which is similar to artificial viscosity. This approach is commonly used in SPH. This study

employs the artificial resistivity proposed by Price,<sup>41</sup> which helps stabilize the simulation when magnetic field discontinuities caused by shocks are present,

$$\left(\frac{d\mathbf{B}_i}{dt}\right)_{diss} = \rho_i \sum_j m_j \frac{\alpha_B v_{sig}^B}{2\bar{\rho}_{ij}^2} (\mathbf{B}_i - \mathbf{B}_j) \hat{\mathbf{r}}_{ij} \cdot \nabla W_{ij}, \quad (21)$$

where  $v_{sig}^B$  is the averaged Alfvén speed,  $\hat{\mathbf{r}}_{ij}$  is the unit vector in the  $\mathbf{r}_{ij}$ , and  $\alpha_B$  is the artificial resistivity coefficient set using the switch described in Tricco and Price,<sup>42</sup>

$$\alpha_B = \min\left(\frac{h|\nabla \mathbf{B}|}{|\mathbf{B}|}, 1\right). \quad (22)$$

#### D. Adaptive SPH method

In SPH simulations involving shockwaves with expansion, the spacing between particles rapidly changes, leading to "particle inconsistency," where the smoothing length does not comprise a sufficient number of particles. This problem can significantly affect the accuracy of SPH simulations.<sup>43</sup> Various methods have been proposed to solve this particle inconsistency problem,<sup>43–46</sup> such as adaptive SPH (ASPH). ASPH is a method wherein a different smoothing length is applied to each particle to increase the accuracy of the SPH approximation in a situation where the spacing between particles changes, as shown in Fig. 1. In the pinch plasma simulation, this ASPH application is essential because the distance between particles can rapidly increase or decrease due to explosion or implosion due to shock.

This study utilizes the ASPH method proposed by Owen<sup>47</sup> to adjust the smoothing length of particles based on the number of particles in the original search range. If excess particles are present, the search range is narrowed to improve the computational speed. On the other hand, if too few particles are present, the search range is widened to solve the particle inconsistency problem, which can reduce the calculation accuracy. This process is performed by defining and using a reference density value,<sup>48,49</sup>

$$\rho_{ref} = m \left(\frac{\sigma}{h}\right)^d, \quad (23)$$

where  $d$  is the system dimension, and  $\sigma$  is a parameter specifying the smoothing length in units of average particle spacing  $(m/\rho)^{1/d}$ , which is 1.2 herein. To select an appropriate smoothing length, the below iteration process is used to compare the reference density with the density derived from the SPH calculation. This iteration is repeated until the difference between the two smoothing lengths  $h_k$  and  $h_{k+1}$  converges below a specified criterion. The smoothing length  $h$  is updated in each iteration using the following formula:

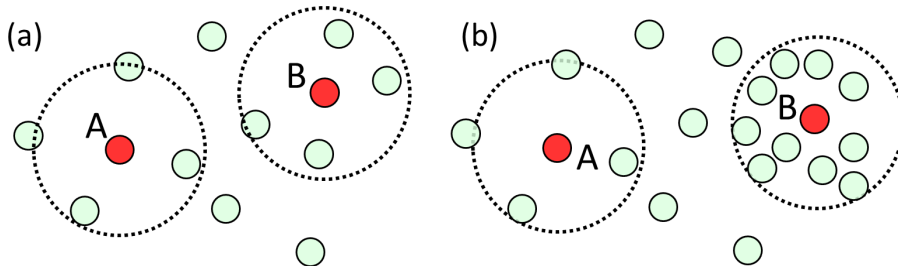


**FIG. 1.** Schematic diagram of particle kernel radius in non-uniform particle distribution (a) before applying ASPH and (b) after applying ASPH.

$$h_{k+1} = h_k - \frac{\partial h_k}{\partial \rho} \rho_{ref}(h_k) - \frac{\rho(h_k)}{1 - \frac{\partial h_k}{\partial \rho} \sum_j m_j \frac{\partial W(h_k)}{\partial h_k}}, \quad (24)$$

$$\frac{\partial h}{\partial \rho} = -\frac{1}{d} \frac{h}{\rho}, \quad (25)$$

$$\frac{\partial W}{\partial h} = -\frac{r}{h} \nabla W - \frac{d}{h} W. \quad (26)$$

To account for the changes in the smoothing length, a smoothing length gradient correction factor  $\Omega$  is used, which is determined as follows:

$$\Omega = 1 - \frac{\partial h_k}{\partial \rho} \sum_j m_j \frac{\partial W(h_k)}{\partial h_k}. \quad (27)$$

The variable  $\Omega$  is applied to Eqs. (13)–(16) to account for the changes in the smoothing length. This correction is important as it ensures the calculation accuracy with varying smoothing length. For example, if ASPH is applied to Eq. (14), it is converted into the following equation:

$$\frac{d\mathbf{v}_i}{dt} = \sum_j m_j \left( \frac{\tilde{\mathbf{M}}_i}{\Omega_i \rho_i^2} \cdot \nabla_i W_{ij} + \frac{\tilde{\mathbf{M}}_j}{\Omega_j \rho_j^2} \cdot \nabla_j W_{ij} \right). \quad (28)$$

## E. Non-ideal MHD terms of the SPH method

To calculate the non-ideal MHD term in the resistive MHD, the current density  $\mathbf{J}$  needs to be accurately calculated first. Previous SPMHD studies calculated the current density via the following two ways:

$$\mathbf{J}_i = -\frac{1}{\rho_i} \sum_j m_j (\mathbf{B}_i - \mathbf{B}_j) \times \nabla_i W_{ij}, \quad (29)$$

$$\mathbf{J}_i = -\rho_i \sum_j m_j \left( \frac{\mathbf{B}_i}{\rho_i^2} + \frac{\mathbf{B}_j}{\rho_j^2} \right) \times \nabla_i W_{ij}. \quad (30)$$

For example, to obtain the current density, Wurster used the difference operator of Eq. (29), and Price used the symmetric operator of Eq. (30).<sup>50</sup> In this study, a more suitable SPH formulation is employed to calculate the current density under pinch plasma conditions,

wherein a large magnetic field discontinuity can occur. A detailed explanation of this process is provided in Sec. IV.

The flexibility of SPH approximations enables a diverse set of constructions, and the SPH formula for the non-ideal MHD term has also been used in various ways. For instance, Bonafede *et al.*<sup>51</sup> and Tsukamoto *et al.*<sup>23</sup> addressed this term by directly taking the second derivatives of the magnetic field. Wurster<sup>52</sup> computed this term by applying a curl calculation to the current density. However, it is unclear which of the two approaches has numerical advantages when using SPH for simulations involving the non-ideal MHD term.<sup>52</sup> Further investigation and comparison between the two methods are necessary to determine the approach that is more accurate or efficient in practical applications. Basically, the first derivative of the current density is computed first using symmetric and difference operators. An “inter-particle” formulation<sup>53</sup> that is known to be effective between two phases with significantly different properties is adopted. Consequently, the SPH code developed in this study is equipped with four types of derivatives for the non-ideal MHD term (i.e., symmetric, difference, Laplacian, and inter-particle), and the derivative forms are summarized in Table II. The impact of the derivative forms of the non-ideal MHD term is shown in Sec. IV.

## F. Time integration

In this study, a modified predictor–corrector time-stepping scheme<sup>54</sup> is applied. The predictor–corrector scheme divides the time integration into two steps as follows: first, the prediction step extrapolates the physical variables (e.g., velocity, position, density, magnetic field, and internal energy) as follows:

$$\mathbf{v}_{t+\frac{\Delta t}{2}}^p = \mathbf{v}_t + \frac{\Delta t}{2} \left( \frac{d\mathbf{v}}{dt} \right)_t, \quad (31)$$

$$\rho_{t+\frac{\Delta t}{2}}^p = \rho_t + \frac{\Delta t}{2} \left( \frac{d\rho}{dt} \right)_t, \quad (32)$$

$$\mathbf{B}_{t+\frac{\Delta t}{2}}^p = \mathbf{B}_t + \frac{\Delta t}{2} \left( \frac{d\mathbf{B}}{dt} \right)_t, \quad (33)$$

$$u_{t+\frac{\Delta t}{2}}^p = u_t + \frac{\Delta t}{2} \left( \frac{du}{dt} \right)_t, \quad (34)$$

where  $\Delta t$  is the time step, and the superscript p denotes “predictor.” The time derivatives of velocity, density, magnetic field, and internal

TABLE II. Four types of SPH derivatives for the non-ideal MHD term.

SPH discretization	SPH Formulation
Symmetric	$\left( \frac{d\mathbf{B}}{dt} \right)_{\text{non-ideal}} = \rho_i \sum_j m_j \left( \frac{\eta_i \mathbf{J}_i}{\rho_i^2} + \frac{\eta_j \mathbf{J}_j}{\rho_j^2} \right) \times \nabla_i W_{ij}$
Difference	$\left( \frac{d\mathbf{B}}{dt} \right)_{\text{non-ideal}} = -\frac{1}{\rho_i} \sum_j m_j (\eta_i \mathbf{J}_i - \eta_j \mathbf{J}_j) \times \nabla_i W_{ij}$
Laplacian	$\left( \frac{d\mathbf{B}}{dt} \right)_{\text{non-ideal}} = \sum_j \frac{4\eta_i \eta_j}{\eta_i + \eta_j} \frac{m_j}{\rho_j} (\mathbf{B}_i - \mathbf{B}_j) \frac{\mathbf{r}_{ij} \cdot \nabla_i W_{ij}}{ \mathbf{r}_{ij} ^2}$
Inter-particle	$\left( \frac{d\mathbf{B}}{dt} \right)_{\text{non-ideal}} = -\frac{\rho_i}{m_i} \sum_j \left( \frac{m_i^2}{\rho_i^2} + \frac{m_j^2}{\rho_j^2} \right) \frac{\rho_i \eta_j \mathbf{J}_j + \rho_j \eta_i \mathbf{J}_i}{\rho_i + \rho_j} \times \nabla_i W_{ij}$

energy are evaluated by solving Eqs. (31)–(34) using the predicted values. Then, the field variables are re-calculated over the entire time step using the updated time derivatives in the correction step,

$$\mathbf{v}_{t+\Delta t}^c = \mathbf{v}_t + \Delta t \left( \frac{d\mathbf{v}}{dt} \right)_{t+\frac{\Delta t}{2}}, \quad (35)$$

$$\rho_{t+\Delta t}^c = \rho_t + \Delta t \left( \frac{d\rho}{dt} \right)_{t+\frac{\Delta t}{2}}, \quad (36)$$

$$\mathbf{B}_{t+\Delta t}^c = \mathbf{B}_t + \Delta t \left( \frac{d\mathbf{B}}{dt} \right)_{t+\frac{\Delta t}{2}}, \quad (37)$$

$$u_{t+\Delta t}^c = u_t + \Delta t \left( \frac{du}{dt} \right)_{t+\frac{\Delta t}{2}}, \quad (38)$$

where the superscript c denotes “corrector.” These corrected values become the initial values for the next time step.

#### IV. BENCHMARK SIMULATION

In this section, the results of the simulation performed to verify and validate the constructed SPH code are explained. In addition, the simulation results of the on-going X-pinch study are presented. The simulations using the implemented models are conducted for three benchmark cases: (1) Brio and Wu shock tube (ideal MHD), (2) resistive MHD shock tube simulation, and (3) magnetized Noh Z-pinch problem. All simulation results are compared with the simulation results and analytical solutions of some reference Eulerian code.

#### A. Brio and Wu shock tube simulations

The Brio and Wu shock tube problem generalizes the classic hydraulics Sod shock tube to MHD.<sup>55</sup> In the Brio and Wu shock tube, the right and left states are initialized to different values. The components of the anti-parallel magnetic field on the two sides of the initial discontinuity lead to four waves, i.e., fast rarefaction wave, slow compound wave, slow shock wave, and fast shock wave, resulting in complex property distribution. The left and right states are initialized as  $(\rho, v_x, v_y, B_x, B_y, P) = [1, 0, 0, 0.75, 1, 1]$  and  $[0.125, 0, 0, 0.75, -1, 0.1]$ , respectively. This example tests whether the code can accurately represent the shocks, rarefactions, contact discontinuities, and compound structures of MHD. Thus, it has been widely used as a benchmark problem to validate ideal MHD calculations.<sup>40,56</sup> In this study, the “1.5D” Brio and Wu shock tube problem (i.e., 1D but with 2D magnetic and velocity fields) is analyzed with 1000 particles in the range  $x \in [-0.5, 0.5]$ . Four physical quantities (i.e., density, pressure, x,y-directional velocity, internal energy, and magnetic field) of the Brio and Wu shock problem are obtained through the constructed SPH code. Figure 2 depicts the simulation results of the Brio and Wu shock tube at 0.1 s. In the figure, the black dots represent the physical quantities of all the particles and the red lines represent the numerical solution obtained using a proven Riemann solver.<sup>57</sup> The results show that the proposed SPH code yields numerically accurate simulations of the ideal MHD problem.

The effect of numerical techniques, such as the correction terms to satisfy the  $\nabla \cdot \mathbf{B}$  constraints and artificial dissipation terms to handle shocks through this problem, is also verified. Figure 3 shows that the

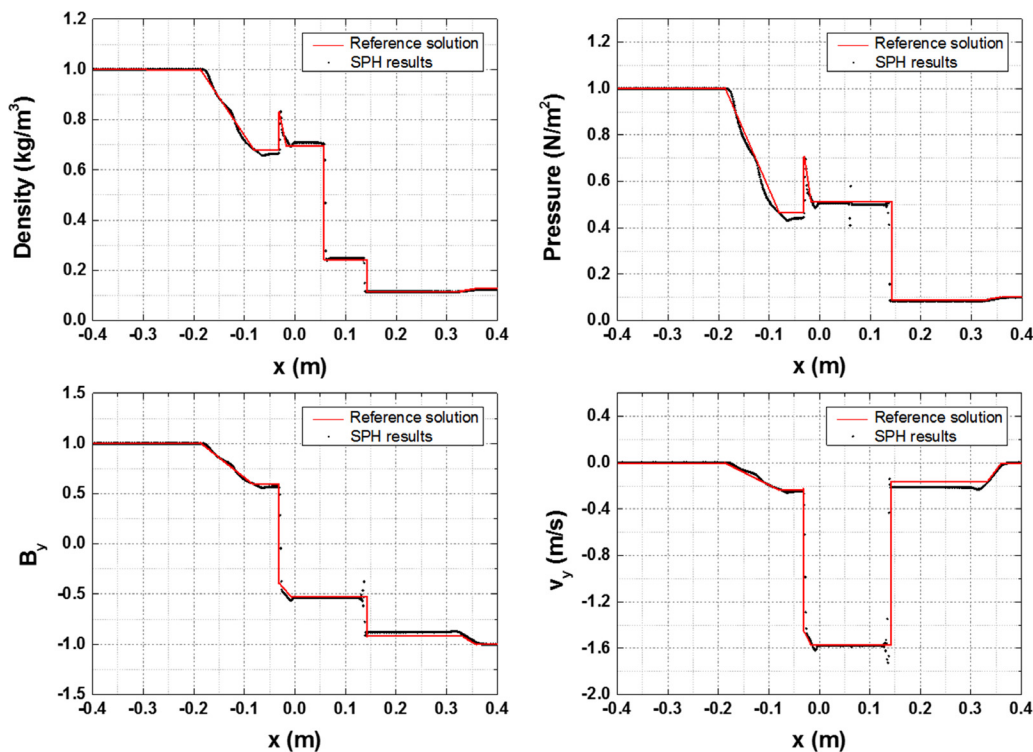


FIG. 2. Brio and Wu shock tube simulation results.

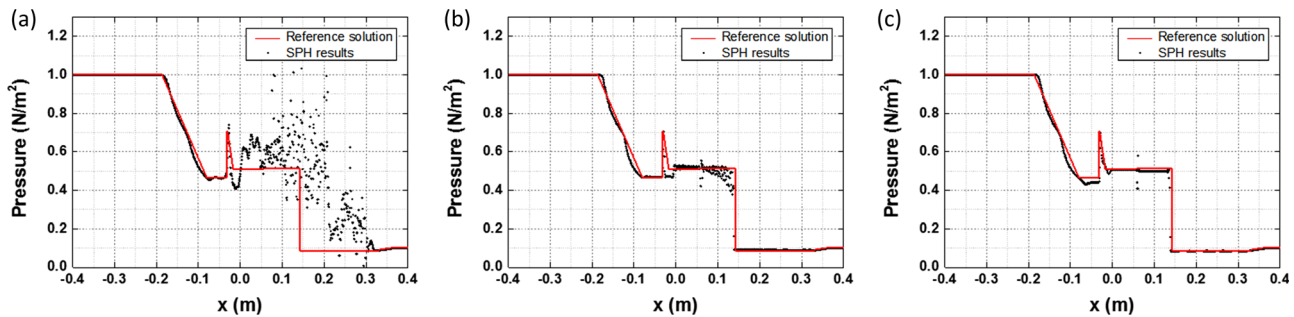


FIG. 3. The pressure field profiles of Brio and Wu shock tube simulation (a) before applying any correction terms, (b) after applying the  $\nabla \cdot \mathbf{B}$  correction term, and (c) artificial resistivity term.

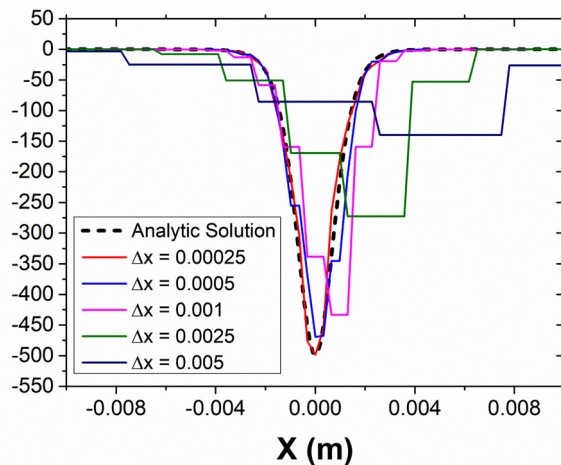


FIG. 4. Effects of particle resolution on SPH current density profiles in resistive MHD shock tube simulation. This sensitivity analysis of particle resolution demonstrates that a sufficiently high resolution is required to capture the sharp peak in current density.

applied numerical treatments are effective. First, whether the numerical instability caused by the  $\nabla \cdot \mathbf{B}$  constraint can be effectively controlled is determined by introducing Eq. (18). The comparison of Figs. 3(a) and 3(b) shows that various numerical errors are removed after the introduction of the correction term. Figure 3(c) displays the calculation results obtained after the incorporation of the artificial resistivity of Eq. (21) into the result of Fig. 3(b). As shown in the figure, the dissipation term for the magnetic field partially controls the existing numerical instability.

## B. Resistive MHD shock tube simulations

In actual pinch plasma simulations, the effect of plasma resistivity on plasma behavior must be considered. Therefore, the resistive term is added in the induction and energy equations. Additionally, the current density needs to be calculated to derive these resistive terms. To verify the accurate functioning of these added terms, resistive MHD shock tube simulations are performed, wherein plasma resistivity is distributed in the ideal MHD shock tube, which is represented by the Brio and Wu shock tube. The left and right states are initialized as  $(\rho^L, v_x^L, P^L) = [1, 0, 1]$  and  $(\rho^R, v_x^R, P^R) = [0.125, 0, 0.1]$ , respectively.

To calculate the exact peak value of the current density, the initial magnetic field is applied as the following steep sigmoidal function:

$$B_y = \frac{0.5 - 0.5 \exp(x/d)}{1 + \exp(x/d)}, \quad (39)$$

where  $d$  is the value that determines the magnetic field gradient in the steep region, which is 0.0005 m herein. In this case, the peak value of current density is 500. Here, high resolution is required to capture the sharp current density peak. Therefore, a sensitivity analysis of the particle resolution is performed, and the result is shown in Fig. 4. Subsequently, simulations are conducted with the particle spacing of 0.00025 m, which is four times closer than that in the Brio and Wu shock tube.

Figure 5 presents the SPH current density profiles of the resistive MHD shock tube simulations. As described in Sec. III E, two types of SPH discretization are used to compute the current density. Figure 5 clearly shows that the current peak at  $x = 0$  is underestimated when the symmetric operator is employed. This tendency becomes more pronounced as the discontinuity of the magnetic field at the interface becomes steeper. Figure 6 displays the current profile when  $d$  is 0.00005 m. In this case, the difference operator well captures the current peak and the symmetric operator yields an additional nonphysical current peak. These results emphasize the importance of using the correct discretization method to obtain accurate results at the discontinuous interface of pinch plasmas.

To accurately model the non-ideal MHD effects in the simulation, investigations are conducted to identify the appropriate SPH discretization form for this term. The plasma resistivity is simulated as a function of density ( $\eta = 10^{-3} \rho^{-6}$ ), and the results are evaluated via comparison with the data from a reference Euler code (PLUTO code<sup>10</sup>). As mentioned in Sec. III E, four types of SPH formulations are considered for the non-ideal MHD term. Figure 7(a) displays the time derivative of the magnetic field obtained using each of the four discretization methods at  $t = 0.0002$  s. Nonphysical oscillations can be observed in the time derivative of the magnetic field for some SPH discretization types. These oscillations grow over time and have a significant negative impact on the computational accuracy. Figure 7(b) shows the difference between the simulation results and the reference data. The figure shows that the inter-particle type of non-ideal MHD term is the most effective in reducing the current density noise stemming from the discretization of the initial large magnetic field discontinuity. This methodology is expected to be effective for various types of

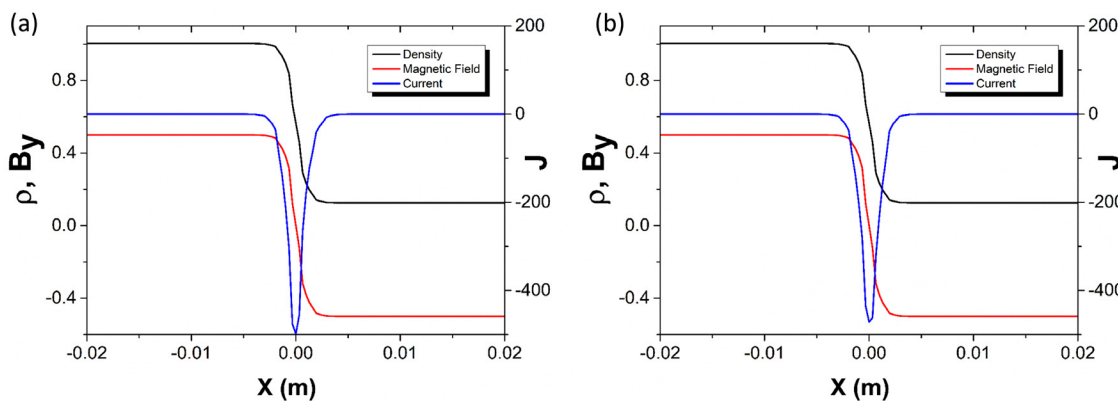


FIG. 5. SPH current density profiles of resistive MHD shock tube simulation using (a) difference operator and (b) symmetric operator ( $d = 0.0005$ ).

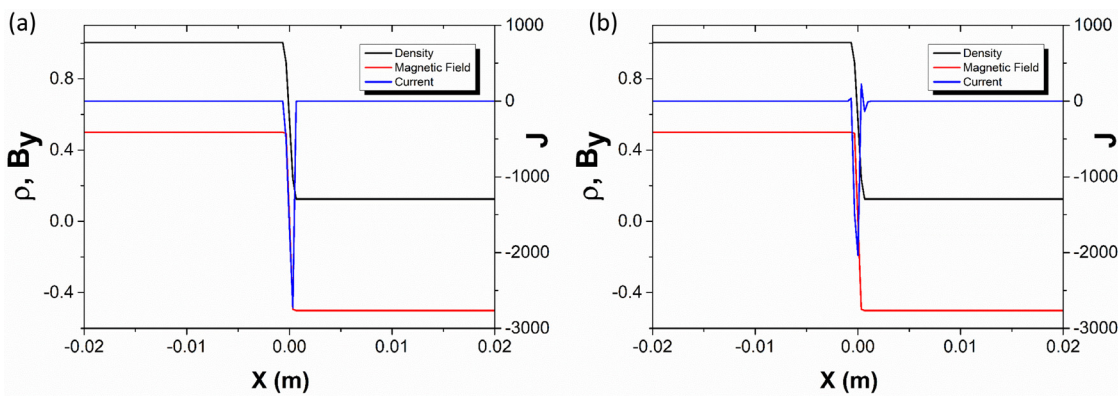


FIG. 6. SPH current density profiles of resistive MHD shock tube simulation using (a) difference operator and (b) symmetric operator ( $d = 0.00005$ ).

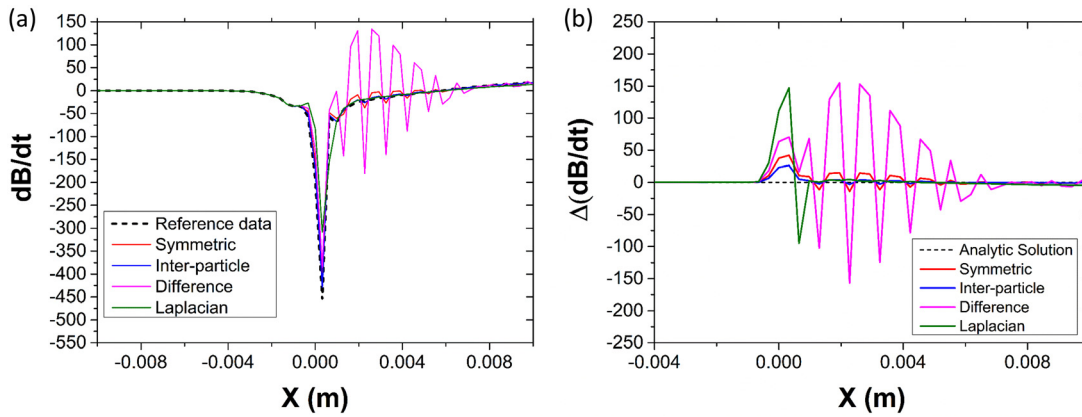


FIG. 7. (a) Time derivative of magnetic field according to the SPH discretization and (b) deviation from reference data at  $t = 0.0002$  s.

pinch plasmas accompanied by discontinuous magnetic fields and resistivities.

### C. Magnetized Noh Z-pinch problem

Velikovich *et al.* proposed the magnetized Noh problem as an example for verifying the pinch plasma analysis ability.<sup>7</sup> The Noh

problem has been used for many years to verify codes designed to deal with implosions, such as in inertial confinement fusion to investigate the hydrodynamic component of MHD codes. The extension of this classic gas dynamics Noh problem to the electromagnetic problem is known as the magnetized Noh Z-pinch problem. The operation of a Z-pinch is very simple. A current driven through the cylindrical

column of the plasma causes the material to rapidly compress axially through the  $\mathbf{J} \times \mathbf{B}$  force. To simulate this multi-dimensional pinch plasma, an initial plasma state is considered that is defined as a function of  $r$ , which represents the distance from the central point. The initial properties of plasma including the density ( $\rho$ ), radial velocity ( $v_r$ ), toroidal magnetic field ( $B_\phi$ ), and plasma pressure ( $P$ ) are  $\rho = 3.1831 \times 10^{-5} r^2 \text{ g/cm}^3$ ,  $v_r = -3.24101 \times 10^7 \text{ cm/s}$ ,  $B_\phi = 6.35584 \times 10^8 r \text{ G}$ , and  $P = \beta \times B_\phi^2$ , respectively. Here, the ratio of the plasma pressure and magnetic pressure ( $\beta$ ) is  $8\pi \times 10^{-6}$ .

The SPH particles are arranged with spacings of 0.01 cm on a 2D plane in the range of  $-3 \text{ cm} < x < 3 \text{ cm}$  and  $-3 \text{ cm} < y < 3 \text{ cm}$ . For the boundary condition, an approach similar to that in a previous study is followed.<sup>7</sup> Specifically, the outermost 10 layers of particles are assigned as boundary particles, and the physical properties of the last layer of plasma particles are copied. Accordingly, the  $\rho$ ,  $v_r$ ,  $B_\phi$ , and  $P$  values of the boundary particle satisfy the zero gradient condition at  $r_{\text{out}} (= 3 \text{ cm})$ . This approach is effective because the boundary is far enough from the center of the plasma, preventing significant influence on the internal dynamics within the first 30 ns of the simulation.

During the simulation, the plasma undergoes temporal evolution, which leads to a significant change in its properties. Therefore, a

crucial criterion for determining the effectiveness of the MHD code for simulating multi-dimensional pinch plasma is its ability to reproduce the self-similar solution<sup>7</sup> for this problem. To evaluate the code's accuracy, the problem is simulated and the density, velocity, and pressure of the plasma at 30 ns are analyzed.

Through this 2D simulation, the application effect of the introduced ASPH method is confirmed. Figure 8(b) presents the comparison of the analytic solution and the simulation result obtained through the SPH code before the ASPH application. As shown in the figure, the peak value of physical properties in the compressed region significantly differs from that in the analytic solution. Two factors contribute to this error. First, the smoothing length at the center point is too large. As shown in Fig. 9(a), the strong compression by the magnetic field causes the particles to gather with a high number density at the central point. If ASPH is not applied, the initial smoothing length used in the simulation may be too large to yield a high number density. Previous studies using Eulerian codes<sup>7</sup> have reported that physical variables are underestimated when the mesh is not dense enough in the magnetized Noh problem. Similarly, in the SPH simulations, an excessively wide smoothing length relative to the particle number density results in the underestimation of physical quantities at the peak point. Second,

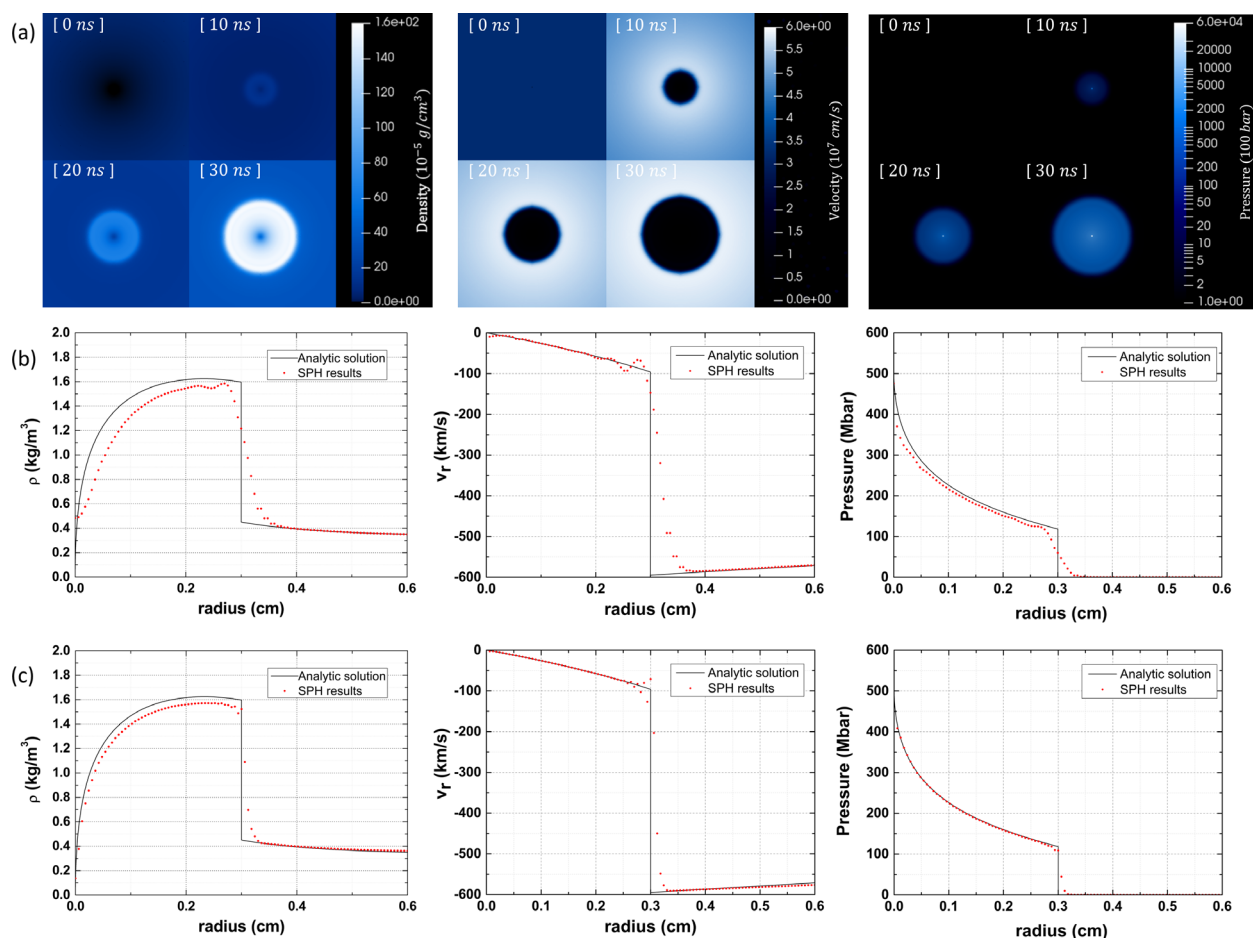


**FIG. 8.** Magnetized Noh simulation results from two-dimensional SPH code: (a) the time evolution of density, velocity, and pressure distributions, and the profiles of the variables (b) before and (c) after applying ASPH. The solid curve is the self-similar solution at 30 ns to the magnetized Noh problem.

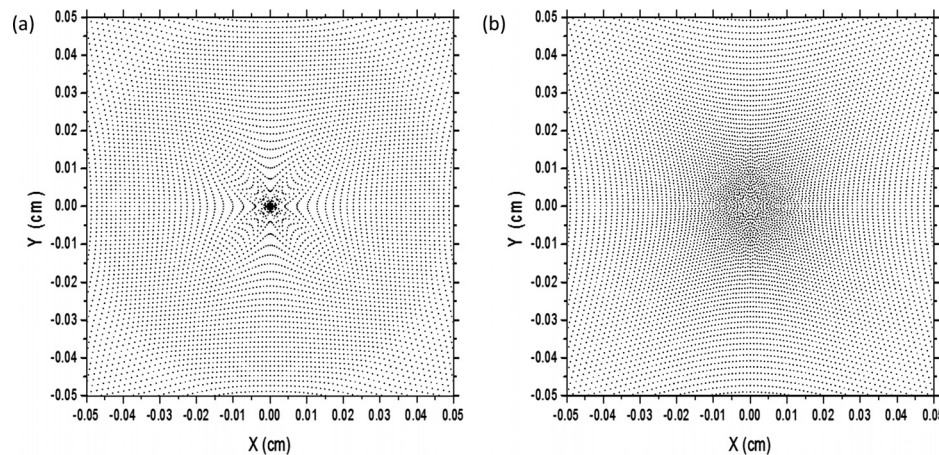


**FIG. 9.** Particle arrangement in magnetized Noh simulation (a) before and (b) after applying ASPH.

tensile instability during the simulation is observed. As shown in Fig. 9(a), during the simulation of the magnetized Noh problem, the particles aggregated and assembled in the same direction. These particle arrangements are known to cause tensile instability, which is accompanied by significant numerical errors in SPH simulations.<sup>58</sup> For the above problems, significant improvement has been achieved through the application of the ASPH method. Figure 8(c) shows the comparison between the simulation results with the ASPH method applied and the analytic solution for the magnetized Noh problem. The figure shows that the accuracy of the SPH code greatly improves in the compression problems after the application of the ASPH method. In addition, as shown in Fig. 9(b), the existing tensile instability is successfully removed due to the application of the ASPH method.

## V. X-PINCH SIMULATION

The simulations for 3D X-pinch are performed using the SPH code verified through the problems in Sec. IV. The X-pinch is an enticing option for small-scale experimentation, as it can produce x-rays using a modest amount of current.<sup>59</sup> X-pinch plasma forms when a fast-rising current of a few hundred kA is applied to two or more thin metallic wires that are mounted in such a way that they cross and touch at a single point in the form of an “X.” In general, a magnetic field forms in the shape of a concentric circle with the wire as the central axis. However, near the cross point, the “global magnetic field” is

dominant because the wires are too close to allow field reversal to occur between them.<sup>1,17,60</sup> This magnetic field distribution generates the characteristic shape of X-pinch, such as (1) micro Z-pinch generated by strong compression at the cross point and (2) plasma jet, which is a plasma transport in the axial direction.

To simulate the central part dominated by the global magnetic field, a counterclockwise magnetic field that is proportional to the distance from the central axis is applied as an initial condition. The electrical current used in the simulations has a constant waveform with a value of 100 kA after the current start. The X-pinch wires are set at a cross angle of 90°. In addition, the X-pinch simulation assumes that the ablation and expansion of the 40-μm-thick copper wires progress and exist in a plasma state. To effectively capture the HED plasma characteristics discussed in Sec. II B in the X-pinch simulation, the EOS based on the Lee–More model is employed.<sup>29</sup> Figure 10 demonstrates that under the conditions of high temperature and density, the plasma exhibits very high conductivity (i.e., very low resistivity). This simulation enables us to assess the operability of the proposed SPH model in these extreme regimes.

Figure 11 displays the implosion behavior of X-pinch plasma, and Fig. 12 presents the velocity profile of the crossed wire plane. In the early stages of the simulation (0–10 ns), the magnetic field compresses the plasma, causing the density at the cross point to rapidly increase. This leads to a high-pressure region at the center of the

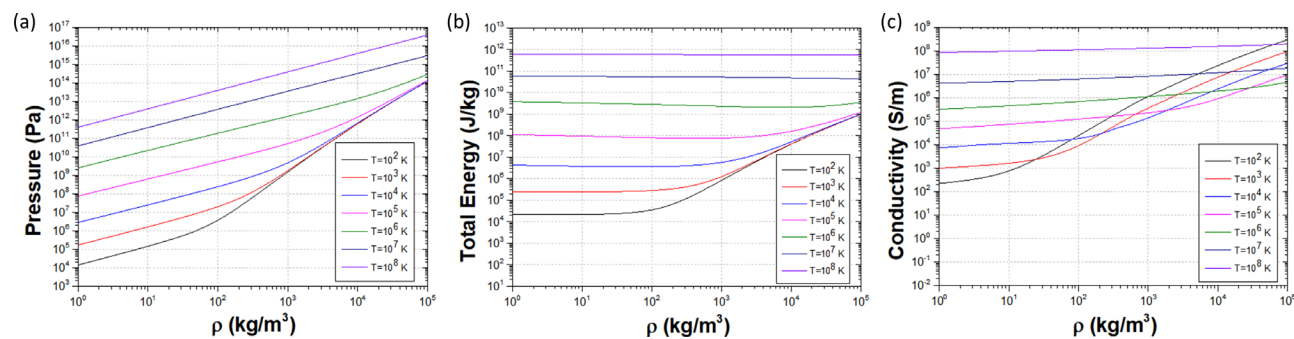


**FIG. 10.** Physical properties of copper plasma computed by the Lee–More EOS model at different temperatures and densities: (a) pressure, (b) total internal energy, and (c) conductivity.

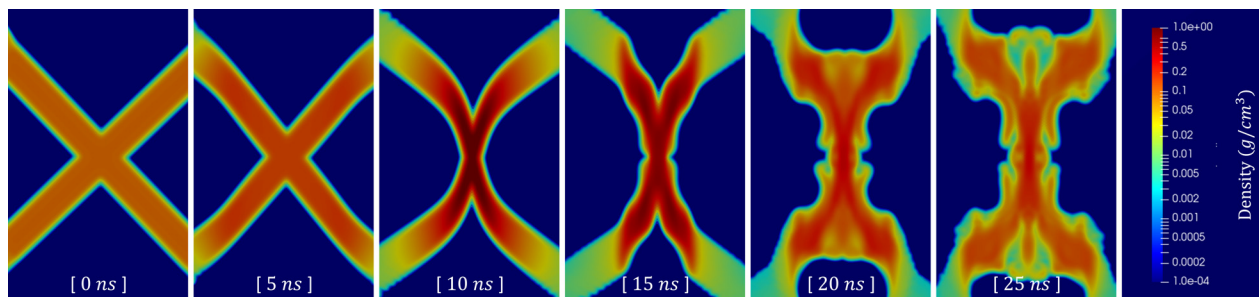


**FIG. 11.** Time evolution of density distribution in X-pinch simulations. Plasma compression by the magnetic field causes a rapid increase in density at the cross point (0–15 ns), resulting in jet formation (15–20 ns). This vertical plasma transport becomes dominant (20 ns onward).

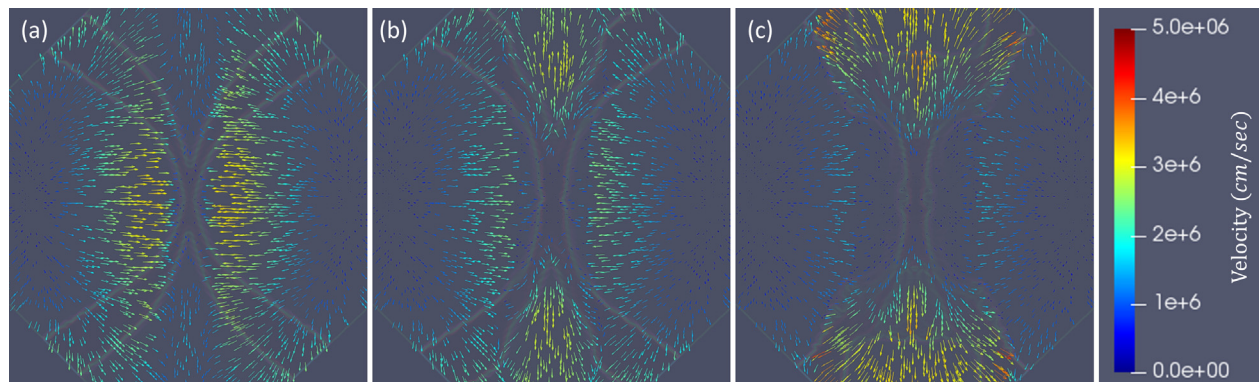
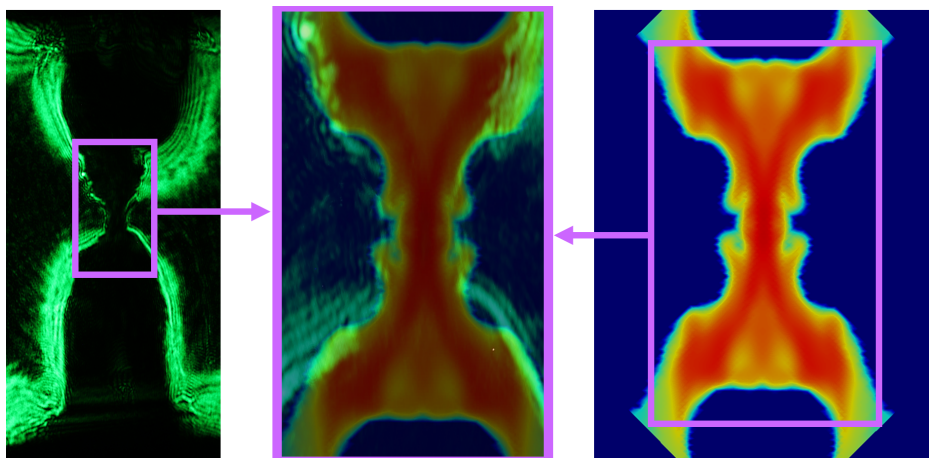


**FIG. 12.** Velocity profile of X-pinch simulations at (a) 10, (b) 15, and (c) 20 ns.



compressed plasma (10–15 ns), and it generates an expansive force. Subsequently, as the compression force and the expansion balance each other, a plasma transport is observed in the vertical direction (referred to as a jet) (15–20 ns). Thereafter ( $>20$  ns), the jet becomes dominant, as shown in Fig. 12(c). This overall behavior is illustrated in Figs. 11 and 12. Schlieren images before and after the discharge are obtained using the experimental setup employed in a previous X-pinch study.<sup>61</sup> Figure 13 presents a comparison between the simulation image and the

Schlieren images captured during the preliminary experiment. The simulation accurately reproduces X-pinch plasma's characteristic neck and beam shape.

## VI. CONCLUSION

In this study, a resistive MHD model was derived for simulating electrically conducting fluids, especially pinch plasma. It is implemented as an SPH code. This non-ideal MHD code was configured by

sequentially adding terms necessary for pinch simulation to the existing SPH-based hydrodynamics code. For the model validation, three benchmark simulations were performed using the implemented code: (1) Brio and Wu shock tube (ideal MHD), (2) resistive MHD shock simulation, and (3) magnetized Noh Z-pinch problem. The simulation results were compared with the reference data. The simulations results quantitatively and qualitatively showed that the constructed SPH code well simulates the behavior of plasmas, including a simple Z-pinch problem. Finally, an X-pinch analysis was performed with this validated code, and the implosion behavior of X-pinch plasma was simulated. The simulation well produced the micro Z-pinch and jet shapes, which are important features of X-pinch plasma.

To improve the accuracy of the proposed X-pinch simulations and compare their results with experimental data, the following studies will be conducted in the future: (1) addition of a radiation model to the SPH code to account for the energy loss through x-ray emission; (2) incorporation of the rigorous plasma property models, such as the EOS model and the plasma conductivity model, specific to X-pinch conditions; and (3) expansion of the energy equation to a two-temperature equation that separates the energies of ions and electrons. After integrating these models, rigorous X-pinch simulations will be conducted and the results will be compared with both experimental data and the results of existing simulations to validate the accuracy of the proposed method.

## ACKNOWLEDGMENTS

This work was supported by the Defense Research Laboratory Program of the Defense Acquisition Program Administration and the Agency for Defense Development of Republic of Korea.

## AUTHOR DECLARATIONS

### Conflict of Interest

The authors have no conflicts to disclose.

### Author Contributions

**Su-San Park:** Conceptualization (lead); Data curation (lead); Formal analysis (equal); Investigation (lead); Methodology (equal); Resources (equal); Software (equal); Validation (lead); Visualization (lead); Writing – original draft (lead); Writing – review & editing (lead).

**Deok-Kyu Kim:** Conceptualization (supporting); Data curation (supporting); Formal analysis (equal); Investigation (supporting); Methodology (supporting); Project administration (equal); Validation (supporting); Writing – review & editing (supporting).

**Jin-Hyun Kim:** Investigation (supporting); Methodology (supporting). **Eung Soo Kim:** Conceptualization (supporting); Formal analysis (equal); Funding acquisition (lead); Methodology (equal); Project administration (equal); Resources (equal); Software (equal); Supervision (lead); Visualization (supporting); Writing – review & editing (supporting).

## DATA AVAILABILITY

The data that support the findings of this study are available from the corresponding author upon reasonable request.

## REFERENCES

- <sup>1</sup>J. P. Chittenden, R. Aliaga Rossel, S. V. Lebedev, I. H. Mitchell, M. Tatarakis, A. R. Bell, and M. G. Haines, “Two-dimensional magneto-hydrodynamic modeling of carbon fiber Z-pinch experiments,” *Phys. Plasmas* **4**, 4309 (1997).
- <sup>2</sup>S. A. Pikuz, T. A. Shelkovenko, V. M. Romanova, D. B. Sinars, D. A. Hammer, S. N. Bland, and S. V. Lebedev, “X pinch as a source for x-ray radiography,” *Nukleonika* **46**(1), 21–25 (2001); available at [http://www.ichtj.waw.pl/ichtj/nukleon/back/full/vol46\\_2001/v46n1p021f.pdf](http://www.ichtj.waw.pl/ichtj/nukleon/back/full/vol46_2001/v46n1p021f.pdf)
- <sup>3</sup>R. K. Appartaim and B. T. Maakuu, “X-pinch x-ray sources driven by a 1  $\mu$ s capacitor discharge,” *Phys. Plasmas* **15**, 072703 (2008).
- <sup>4</sup>A. Skoulakis, G. Koundourakis, A. Ciardi, E. Kaselouris, I. Fililis, J. Chatzakis, M. Bakarezos, N. Vlahakis, N. A. Papadogiannis, M. Tatarakis, and V. Dimitriou, “High performance simulations of a single X-pinch,” *Plasma Phys. Controlled Fusion* **64**(2), 025003 (2022).
- <sup>5</sup>J. Huang, N. Ding, C. Ning, S. Sun, Y. Zhang, D. Xiao, and C. Xue, “Numerical investigation on the implosion dynamics of wire-array Z-pinches in (r, q) geometry,” *Phys. Plasmas* **19**, 062701 (2012).
- <sup>6</sup>P. Tzeferacos, M. Fatenejad, N. Flocke, G. Gregori, D. Q. Lamb, D. Lee, J. Meinecke, A. Scopatz, and K. Weide, “FLASH magnetohydrodynamic simulations of shock-generated magnetic field experiments,” *High Energy Density Phys.* **8**, 322–328 (2012).
- <sup>7</sup>A. L. Velikovich, J. L. Giuliani, S. T. Zalesak, J. W. Thornhill, and T. A. Gardiner, “Exact self-similar solutions for the magnetized Noh Z pinch problem,” *Phys. Plasmas* **19**, 012707 (2012).
- <sup>8</sup>N. Ding, Y. Zhang, D. Xiao, J. Wu, Z. Dai, L. Yin, Z. Gao, S. Sun, C. Xue, C. Ning, X. Shu, and J. Wang, “Theoretical and numerical research of wire array Z-pinch and dynamic hohlraum at IAPCM,” *Matter Radiat. Extremes* **135**(1), 135–152 (2016).
- <sup>9</sup>N. Ding, J. Wu, Z. H. Yang, S. W. Fu, C. Ning, Q. Liu, X. J. Shu, Y. Zhang, and Z. H. Dai, “Simulation of Z-pinch implosion using MARED code,” *High Power Laser Part. Beams* **20**, 212 (2008); available at [https://inis.iaea.org/search/search.aspx?orig\\_q=RN:40095483](https://inis.iaea.org/search/search.aspx?orig_q=RN:40095483)
- <sup>10</sup>A. Mignone, G. Bodo, S. Massaglia, T. Matsakos, O. Tesileanu, C. Zanni, and A. Ferrari, “PLUTO: A numerical code for computational astrophysics,” *Astrophys. J., Suppl. Ser.* **170**(1), 228–242 (2007).
- <sup>11</sup>A. Skoulakis, G. Koundourakis, E. Kaselouris, I. Fililis, E. Bakarezos, E. L. Clark, N. Vlahakis, N. A. Papadogiannis, V. Dimitriou, and M. Tatarakis, “Preliminary computational study of plasma dynamic evolution produced by low current table-top pinch plasma devices,” in *9th GRACM Int. Congress on Computational Mechanics* (GRACM, 2018), pp. 294–303.
- <sup>12</sup>X. G. Wang, S. K. Sun, D. L. Xiao, G. Q. Wang, Y. Zhang, S. T. Zhou, X. D. Ren, Q. Xu, X. B. Huang, N. Ding, and X. J. Shu, “Numerical study on magneto-Rayleigh–Taylor instabilities for thin liner implosions on the primary test stand facility,” *Chin. Phys. B* **28**, 035201 (2019).
- <sup>13</sup>G. Koundourakis, A. Skoulakis, E. Kaselouris, I. Fililis, E. L. Clark, J. Chatzakis, M. Bakarezos, N. Vlahakis, N. A. Papadogiannis, V. Dimitriou, and M. Tatarakis, “A numerical study on laboratory plasma dynamics validated by low current x-pinch experiments,” *Plasma Phys. Controlled Fusion* **62**, 125012 (2020).
- <sup>14</sup>F. N. Beg, A. Ciardi, I. Ross, Y. Zhu, A. E. Dangor, and K. Krushelnick, “Jet formation and current transfer in X-pinches, in,” *IEEE Trans. Plasma Sci.* **34**(5), 2325–2329 (2006).
- <sup>15</sup>J. P. Chittenden, A. Ciardi, C. A. Jennings, S. V. Lebedev, D. A. Hammer, S. A. Pikuz, and T. A. Shelkovenko, “Structural evolution and formation of high-pressure plasmas in X-pinches,” *Phys. Rev. Lett.* **98**, 025003 (2007).
- <sup>16</sup>D. Haas, S. C. Bott, V. Vilkhev, Y. Eshaq, U. Ueda, T. Zhang, E. Baranova, S. I. Krasheninnikov, and F. N. Beg, “Dynamics of low-density coronal plasma in low current x-pinches,” *Plasma Phys. Controlled Fusion* **49**, 1151 (2007).
- <sup>17</sup>G. W. Collins, D. Marsical, D. M. Haas, R. E. Madden, K. Gunasekara, J. Kim, M. L. Abarr, S. C. Bott, J. P. Chittenden, and F. N. Beg, “Effect of the global to local magnetic field ratio on the ablation modulations on X-pinches driven by 80 kA peak current,” *New J. Phys.* **14**, 043021 (2012).
- <sup>18</sup>R. A. Gingold and J. J. Monaghan, “Smoothed particle hydrodynamics: Theory and application to non-spherical stars,” *Mon. Not. R. Astron. Soc.* **181**(3), 375–389 (1977).
- <sup>19</sup>T. S. Tricco and D. J. Price, “Constrained hyperbolic divergence cleaning for smoothed particle magnetohydrodynamics,” *J. Comput. Phys.* **231**, 7214 (2012).

- <sup>20</sup>D. J. Price and J. J. Monaghan, "Smoothed Particle Magnetohydrodynamics—I. Algorithm and tests in one-dimension," *Mon. Not. R. Astron. Soc.* **348**(1), 123–138 (2004).
- <sup>21</sup>K. Iwasaki and S.-I. Inutsuka, "Smoothed particle magnetohydrodynamics with a Riemann solver and the method of characteristics," *Mon. Not. R. Astron. Soc.* **418**(3), 1668–1688 (2011).
- <sup>22</sup>S.-I. Inutsuka, "Reformulation of Smoothed Particle Hydrodynamics with Riemann Solver," *J. Comput. Phys.* **179**, 238 (2002).
- <sup>23</sup>Y. Tsukamoto, K. Iwasaki, and S.-I. Inutsuka, "An explicit scheme for Ohmic dissipation with smoothed particle magnetohydrodynamics," *Mon. Not. R. Astron. Soc.* **434**(3), 2593–2599 (2013).
- <sup>24</sup>L. Vela Vela, R. Sánchez, J. M. Reynolds-Barredo, and J. Geiger, "Magnetohydrodynamical nonlinear simulations of magnetically confined plasmas using smooth particle hydrodynamics (SPH)," *Phys. Plasmas* **26**, 012511 (2019).
- <sup>25</sup>Y. B. Jo, S. H. Park, H. Y. Choi, H. W. Jung, Y. J. Kim, and E. S. Kim, "SOPHIA: Development of Lagrangian-based CFD code for nuclear thermal-hydraulics and safety applications," *Ann. Nucl. Energy* **124**, 132–149 (2019).
- <sup>26</sup>H. Alfvén, "Existence of electromagnetic-hydrodynamic waves," *Nature* **150**(3805), 405–406 (1942).
- <sup>27</sup>T. Boyd and J. Sanderson, "Resistive magnetohydrodynamics," in *The Physics of Plasmas* (Cambridge University Press, Cambridge, 2003), pp. 140–196.
- <sup>28</sup>M. N. Saha, "LIII. Ionization in the solar chromosphere," *Philos. Mag. Ser.* **6** **40**(238), 472–488 (1920).
- <sup>29</sup>D.-K. Kim and I. Kim, "Calculation of ionization balance and electrical conductivity in nonideal aluminum plasma," *Phys. Rev. E* **68**, 056410 (2003).
- <sup>30</sup>A. Kemp and J. Meyer-ter-Vehn, "An equation of state code for hot dense matter, based on the QEOS description," *Nucl. Instrum. Methods Phys. Res., Sect. A* **415**(3), 674–676 (1998).
- <sup>31</sup>R. M. More, "Pressure ionization resonances and the continuity of bound and free states," *Adv. At. Mol. Phys.* **21**, 305 (1985).
- <sup>32</sup>G. R. Liu and M. B. Liu, *Smoothed Particle Hydrodynamics: A Meshfree Particle Method* (World Scientific, 2003).
- <sup>33</sup>W. Dehnen and H. Aly, "Improving convergence in smoothed particle hydrodynamics simulations without pairing instability," *Mon. Not. R. Astron. Soc.* **425**(2), 1068–1082 (2012).
- <sup>34</sup>S. Børve, M. Omang, and J. Trulsen, "Two-dimensional MHD smoothed particle hydrodynamics stability analysis," *Astrophys. J., Suppl. Ser.* **153**, 447–462 (2004).
- <sup>35</sup>J. M. Stone and T. A. Gardiner, "Athena: A new code for astrophysical MHD," *Astrophys. J., Suppl. Ser.* **178**, 137 (2008).
- <sup>36</sup>J. Wurster, D. J. Price, and M. R. Bate, "Can non-ideal magnetohydrodynamics solve the magnetic braking catastrophe?," *Mon. Not. R. Astron. Soc.* **457**, 1037–1061 (2016).
- <sup>37</sup>S. Børve, M. Omang, and J. Trulsen, "Regularized smoothed particle hydrodynamics: A new approach to simulation magnetohydrodynamic shocks," *Astrophys. J.* **561**, 82–93 (2001).
- <sup>38</sup>W. F. Noh, "Errors for calculations of strong shocks using an artificial viscosity and an artificial heat flux," *J. Comput. Phys.* **72**(1), 78–120 (1987).
- <sup>39</sup>M. L. Wilkins, "Use of artificial viscosity in multidimensional fluid dynamic calculations," *J. Comput. Phys.* **36**(3), 281–303 (1980).
- <sup>40</sup>J. J. Monaghan and R. A. Gingold, "Shock simulation by the Particle Method SPH," *J. Comput. Phys.* **52**(2), 374–389 (1983).
- <sup>41</sup>D. J. Price, "Smoothed particle hydrodynamics and magnetohydrodynamics," *J. Comput. Phys.* **231**(3), 759–794 (2012).
- <sup>42</sup>T. S. Tricco and D. J. Price, "A switch to reduce resistivity in smoothed particle magnetohydrodynamics," *Mon. Not. R. Astron. Soc.* **436**, 2810–2817 (2013).
- <sup>43</sup>M. B. Liu and G. R. Liu, "Restoring particle consistency in smoothed particle hydrodynamics," *Appl. Numer. Math.* **56**(1), 19–36 (2006).
- <sup>44</sup>J. Bonet and S. Kulasegaram, "Correction and stabilization of smoothed particle hydrodynamics method with applications in metal forming simulations," *Int. J. Numer. Methods Eng.* **47**(6), 1189–1214 (2000).
- <sup>45</sup>G. R. Johnson, R. A. Stryk, and S. R. Beissel, "SPH for high velocity impact computations," *Comput. Methods Appl. Mech. Eng.* **139**(1–4), 347–373 (1996).
- <sup>46</sup>P. W. Randles and L. D. Libersky, "Smoothed particle hydrodynamics some recent improvements and applications," *Comput. Methods Appl. Mech. Eng.* **139**(1–4), 375–408 (1996).
- <sup>47</sup>J. M. Owen, J. V. Villumsen, P. R. Shapiro, and H. Martel, "Adaptive smoothed particle hydrodynamics: methodology. II," *Astrophys. J., Suppl. Ser.* **116**(2), 155 (1998).
- <sup>48</sup>D. J. Price and J. J. Monaghan, "Smoothed Particle Magnetohydrodynamics—II. Variational principles and variable smoothing-length terms," *Mon. Not. R. Astron. Soc.* **348**(1), 139–152 (2004).
- <sup>49</sup>J. J. Monaghan, "Smoothed particle hydrodynamics," *Rep. Prog. Phys.* **68**(8), 1703–1759 (2005).
- <sup>50</sup>D. J. Price, "Smoothed particle magnetohydrodynamics - IV. Using the vector potential," *Mon. Not. R. Astron. Soc.* **401**, 1475–1499 (2010).
- <sup>51</sup>A. Bonafede, K. Dolag, F. Stasyszyn, G. Murante, and S. Borgani, "A non-ideal magnetohydrodynamic GADGET: Simulating massive galaxy clusters," *Mon. Not. R. Astron. Soc.* **418**, 2234–2250 (2011).
- <sup>52</sup>J. Wurster, D. Price, and B. Ayliffe, "Ambipolar diffusion in smoothed particle magnetohydrodynamics," *Mon. Not. R. Astron. Soc.* **444**(2), 1104–1112 (2014).
- <sup>53</sup>X. Y. Hu and N. A. Adams, "An incompressible multi-phase SPH method," *J. Comput. Phys.* **227**(1), 264–278 (2007).
- <sup>54</sup>J. C. Butcher, "Numerical methods for ordinary differential equations in the 20th century," *J. Comput. Appl. Math.* **125**(1–2), 1–29 (2000).
- <sup>55</sup>M. Brio and C. C. Wu, "An upwind differencing scheme for the equations of ideal magnetohydrodynamics," *J. Comput. Phys.* **75**, 400–422 (1988).
- <sup>56</sup>S. Vanaverbeke, R. Keppens, S. Poedts, and H. Boffin, "GRADSPH: A parallel smoothed particle hydrodynamics code for self-gravitating astrophysical fluid dynamics," *Comput. Phys. Commun.* **180**(7), 1164–1182 (2009).
- <sup>57</sup>D. S. Balsara, "Total variation diminishing scheme for adiabatic and isothermal magnetohydrodynamics," *Astrophys. J., Suppl. Ser.* **116**(1), 133 (1998).
- <sup>58</sup>T. A. Shelkovenko, S. A. Pikuz, IN. Tilikin, M. D. Mitchell, S. N. Bland, and D. A. Hammer, "Evolution of X-pinch loads for pulsed power generators with current from 50 to 5000 kA," *Matter Radiat. Extremes* **3**(6), 267–277 (2018).
- <sup>59</sup>J. J. Monaghan, "SPH without a tensile instability," *J. Comput. Phys.* **159**(2), 290–311 (2000).
- <sup>60</sup>V. I. Oreshkin, A. P. Artyomov, S. A. Chaikovsky, E. V. Oreshkin, and A. G. Roussikh, "Simulation of the radiation from the hot spot of an X-pinch," *Phys. Plasmas* **24**, 012703 (2017).
- <sup>61</sup>S. C. Bott, D. M. Haas, U. Ueda, Y. Eshaq, R. Madden, G. Collins, and F. N. Beg, "High-resolution laser Schlieren imaging of coronal plasma evolution in 80-kA X-pinches," *IEEE Trans. Plasma Sci.* **36**(4), 1274–1275 (2008).